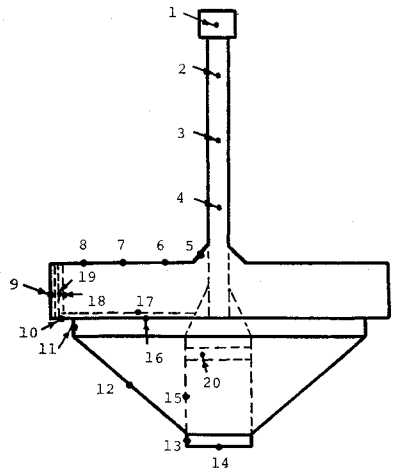

Fig. 1 Nodal breakdown of EPE-D spacecraft.

where $\{J_{im}^{(k)}\}$ is the inverse of the coefficient matrix in the linear systems. Then according to the MRD scheme,

$$\epsilon_m^{(\text{new})} = \epsilon_m^{(\text{old})} - |\partial W/\partial T_{ik}|/(\partial W/\partial T_{ik})\cdot(\partial T_{ik}/\partial \epsilon_m)\Delta S/D \tag{6}$$

where (ΔS) is a suitable and somewhat arbitrary step size that must be chosen small enough for the MRD method to converge to the minimum point. The new α's are found in the same way.

The optimization process can now be executed as follows: 1) make initial estimates of the ϵ_i and α_{Si} $(i = 1,2,\ldots,N)$; 2) calculate the temperatures for every element i and every heating condition k from Eqs. (3) and (4); 3) calculate the worst-case function by Eq. (1); 4) calculate partial derivatives of W by Eqs. (5) and (1); and 5) determine new values of the ϵ_i and α_{Si} from Eq. (6).

This process is repeated until the method fails to improve W for an arbitrarily small ΔS.

Example Application

The application considered is the NASA Explorer XXVI (EPE-D) spacecraft. (Reference 3 also presents an example of a hypothetical cylindrical satellite.) A schematic of the vehicle is presented in Fig. 1 showing the element numbers as used in the analytical model developed at NASA Goddard. Approximately 20 man-days and 4 hr of IBM 7094 computer time were required to "optimize" the coating pattern by the former trial-and-error method. The present method, applied with no foreknowledge of the values obtained at NASA, yielded the results (shown on Table 1) after only 2 man-days and $\frac{1}{2}$ hr of IBM 7094 time. The respective values of W are also shown on this table. The advantages of cost saving and better performance are evident.

Table 1 Summary of EPE-D designs

Node	Allowable Limits	Temperature Ranges - °R: Predicted Limits, Using NASA Coatings	Predicted Limits, Using Present Method
1	420 - 564	468 - 537	478 - 542
6	456 - 600	471 - 600	477 - 572
7	456 - 600	468 - 599	475 - 574
8	456 - 600	470 - 578	482 - 566
17	492 - 546	495 - 535	499 - 540
18	492 - 546	509 - 524	501 - 540
20	474 - 582	488 - 564	517 - 572
	Value of "W"	1.0	0.78

Node	Allowable Limits	Coatings: NASA α	NASA ε	Present Method α	Present Method ε
1		.278	.260	.152	.118
2		.170	.112	.149	.115
3		.170	.112	.153	.116
4		.170	.112	.155	.118
5		.320	.260	.150	.119
6		.310	.240	.167	.196
7		.310	.240	.168	.199
8		.310	.240	.168	.198
9		.970	.850	.207	.166
10		.970	.850	.146	.123
11		.970	.850	.170	.147
12		.160	.110	.163	.183
13		.310	.240	.153	.123
14		.350	.850	.144	.116

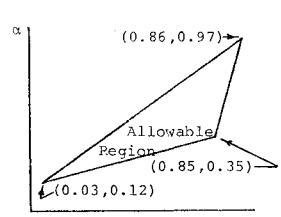

Conclusions

The optimization process outlined above has proven to be a significant improvement over former trial-and-error methods, both in cost and performance. Because of the general nature of the temperature equations used, the method has a wide range of applicability in spacecraft design.

References

[1] Costello, F. A., Harper, T., and Cline, P., "A Rational Approach to the Selection of Satellite Optical Coating Patterns for Temperature Control," preprint 63-HT-41, Aug. 1964, American Society of Mechanical Engineers.

[2] Costello, F. A. et al., "The Optimization of Spacecraft Coating Patterns for Temperature Control," Preprint 67-HT-55. presented at the ASME-AIChE Heat Transfer Conference, Aug. 1967, American Society of Mechanical Engineers.

[3] "Coating Selection Program," Rept. 65SD526, April 15, 1965, General Electric Co., King of Prussia, Pa.; also Rept. CR-1041, NASA.

[4] Costello, F. A. and Schrenk, G. L., "Numerical Solution to the Heat Transfer Equations with Combined Conduction and Radiation," *Journal of Computational Physics*, Vol. 1, No. 4, 1967, p. 541.

Effect of Debris Shielding on Energy Partition

C. H. Lewis* and A. J. Laderman†
Advanced Development Operation,
Aeronutronic Division of Philco-Ford Corporation,
Newport Beach, Calif.

In a recent paper Kuby and Lewis[1] reported on the damage produced by impingement of a cloud of micron-sized aluminum-oxide particles on aluminum targets. Their results indicated that the impingement damage was considerably less than that expected on the basis of single impact data but, although several possible reasons were advanced, no clear explanation was found. Subsequently[2,3] it has been shown that for a wide range of incident particle mass flux, a debris layer is formed immediately ahead of the target, partially shielding it from subsequent impingement by oncoming particles. In the presence of shielding, relative damage, i.e., damage per incident particle, was observed to increase with decreasing particle mass flux, exceeding even that predicted by direct extension of single impact data, while

Table 1 Test results of particle impingement heating

Number of tests	Target material	$\dot{m}_p$, g/cm²-sec	T_0, °K	q_0, cal/cm²-sec	$\dot{T}$, °K/sec	α
3	1100-F	1.3	300	560	140–165	0.080–0.095
3	6061-T6	1.3	300	560	150–170	0.086–0.10
5	1100-F	1.3–1.5	550	1000–1100	230–315	0.065–0.105
3	2024-T3	1.2–1.4	550	900–1000	240–270	0.085–0.095
3	6061-T6	1.2–1.4	550	900–1000	160–215	0.05–0.075

Received July 31, 1969. This work was supported by NASA under JPL Contract 951246.

* Senior Research Engineer, Fluid Mechanics Department. Member AIAA.

† Supervisor, Experimental Fluid Physics Section. Member AIAA.

Table 2 Energy accommodation factors determined from rocket firings[4]

Motor	P_c, psia	Alumina content, %	D_t,[a] cm	D_e,[a] cm	θ, deg	Test: Material	Test: Configuration	Test: Incidence	X_T,[a] cm	q, cal/cm²-sec	α	$\dot{m}_p$, g/cm²-sec
SII ullage	930	8	7.6	30	12	TFE	3.81-cm-diam hemisphere	90°	50	700	0.25	0.08
Minuteman subscale	570	25	1.9	5.9	17	steel and three ablators	flat plate	30,60,90°	1.65	1200–2000	0.11–0.18	5
SPREE	700	23	4.3	12.4	15	not specified	flat plate	90°	37	15–80	0.01–0.07	2
Rohm & Haas	730	31	2.4	7.5	15	copper	blunt body, 3-cm nose radius	90°	5	500	0.09	4.5
Centaur retro (Thiokol TX-3)	1100	4	1.8	3	15	aluminum	flat plate	parallel to and 30 cm from plume axis	100	0.5	0.02	0.1

[a] D_t = throat diameter, D_e = exit-plane diameter, X_T = target, distance from exit plane.

the major constituent of the debris layer shifted from spent projectile material to target ejecta. It was concluded[2] that the debris layer acts as a sink which absorbs a significant fraction of the kinetic energy of the freestream particles, thereby reducing the energy flux to the target. As the incident particle mass flux is reduced, the concentration of debris material decreases, resulting in a greater number of direct impacts and thus an increased energy flux per incident particle. This leads to proportionally more damage per oncoming particle. It is clear, therefore, that the partitioning of the incident energy flux between the target, target ejecta, and rebounded particles depends on the degree of target shielding. This Note describes the results of experiments designed to examine the energy partitioning process under conditions of strong shielding, i.e., when the debris is comprised primarily of spent projectile material.

Tests were performed using the cold-flow facility described in Ref. 1. Aluminum targets were located in the freejet expansion from a nominal Mach 4 nozzle, which used helium to accelerate aluminum-oxide particles. The final particle velocity ranged from 1700 to 2000 m/sec as the helium stagnation temperature was varied from 300 to 500°K. The particles were characterized by a number peak diameter of 1.2 μ and a mass mean diameter of 5 μ. Three aluminum target materials were tested: 1100-0, 6061-T6, and 2024-T3. The targets, which were cylindrical discs 2.54 cm in diameter by 0.31 cm thick, were installed concentric with the nozzle axis and normal to the flow at a distance 0.5 exit diameters (3 cm) from the nozzle exit. The targets were attached at their rear surface to a thermal insulator. A thermocouple was attached to the rear surface of the target to provide a temperature history during the test. For the high-stagnation-temperature tests, the specimen was heated initially to the gas stagnation temperature by a small heating coil mounted in the holder, so that the measured temperature rise would be indicative of particle impaction heating and not of gas stagnation-point heating. The gas was allowed to run for ~1 sec after the conclusion of the particle impaction test to permit an experimental measure of the gas cooling rate. In all cases the temperature variation after the conclusion of the particle flow was at least 50 times smaller than the rate of temperature rise during the duration of particle impaction. Therefore, gas cooling had a negligible effect on the measured target temperature. In addition, since calculations indicated that the temperature gradient across the specimen was small compared to the mean temperature and that the heat loss to the insulator was negligible, the thermocouple reading was assumed to provide directly the instantaneous target temperature.

The specimens were weighed before and after exposure to the particle cloud. The mass loss was typically 0.10 g, or 1% of the initial target mass, which corresponds to a surface regression rate of ~0.005 cm/sec. Although the room temperature shear strengths of the 6061-T6 and 2024-T3 aluminum alloys are several times greater than that of the pure 1100-0 material, no difference in erosion resistance was detected. This result is probably due to the fact that at the elevated temperature produced by the particle impact heating, the shear strengths of the alloys approach that of the pure metal.

The parameter α, defined as the ratio of the particle impact heating rate to the sum of the particle freestream kinetic and thermal energy fluxes, is commonly referred to as the energy accommodation coefficient. In the present experiments, α was calculated from the slope of the recorded temperature history of the target. Since the thermal energy of the particle was negligible compared to its kinetic energy, q_0, and the target mass loss was small compared to its initial mass, α can be expressed as

$$\alpha = \rho_T L C \dot{T} / q_0 \tag{1}$$

where ρ_T is the density, L is the thickness, and C is the specific heat of the target and $\dot{T}$ is the slope of the temperature-time curve. On all tests $\dot{T}$ was nearly constant, indicating that α is essentially constant during the impingement process. In addition, within the accuracy of the measurements, α was independent of target material. Typical run conditions and test results are listed in Table 1. The results show clearly that, in the case of strong shielding, the debris layer acts as an energy barrier, absorbing at least 90% of the kinetic energy flux of incident particle stream. This is in sharp contrast to the typical high-velocity, single-impact process where all of the projectile energy is absorbed by the target with up to 50% appearing as thermal energy, 30% transferred as kinetic energy of the ejecta, and 20% appearing as energy of recrystallization of the target material.

On the basis of the experimental results, it is possible to estimate the temperature of the debris layer. It is assumed that the debris layer is formed in a time small compared to the test duration‡ so that the material within the layer and the flux of particles leaving it are constant. Neglecting target mass loss, we can write

$$q_0 = \rho_T L C \dot{T}_T + \dot{m}_p C_p (T_p - T_i) \tag{2}$$

The energy absorbed by the target, $\rho_T L C \dot{T}_T$, is equal to αq_0; $\dot{m}_p C_p (T_p - T_i)$ is the net thermal energy convected out of the debris layer, T_p is the temperature of the debris material, T_i is the temperature of incident particles, $\dot{m}_p$ is the particle mass flux per unit area, and C_p is the particle specific heat. For $\alpha = 0.1$ and $q_0 = 560$ cal/cm²-sec, $T_p = 1700$°K, while for $q_0 = 1000$ cal/cm²-sec, T_p equals the melting point of alumina, indicating that the debris layer is in a molten state. Since the nominal run duration was 2 sec, the maximum target temperature did not exceed 800°K, so that the target was considerably cooler than the debris layer.

In view of these findings, it is of interest to examine the possible influence of target shielding on the impingement heating which has been determined in other experiments.

‡ Estimates indicate that the formation time is of the order of 10^{-3} sec.

A number of such studies, reported in Ref. 4, are summarized in Table 2, which lists accommodation coefficients determined for several motors together with information on motor geometry and target configuration. Also listed in Table 2 are the incident particle mass fluxes at the target location. These values were not available in Ref. 4 and were calculated from the listed chamber pressure, throat area, and alumina loading by assuming 1) a C^* velocity of 5500 fps and 2) that the particles at the target location were uniformly distributed within the nozzle cone angle. The shock-layer gas density which was determined from plume flowfield data,[4] was approximately 20 times less than that of sea-level air, except for the Centaur motor, where the density was another order of magnitude lower. For each case the particle mass and the shock layer density correspond to the regime of strong debris shielding as identified in Fig. 1 of Ref. 3. It is concluded, therefore, that the process of energy partitioning which occurred on these tests is similar to that described in the present paper. Since the interrelationship between energy partitioning and debris shielding is as yet unknown, the accommodation coefficients listed in Table 2 should be considered valid only for the specified test conditions and should not be applied to situations differing from those for which they were obtained.

In conclusion, the results of the present study show that in the case of strong shielding, the debris layer acts as an efficient energy sink which reduces the net energy flux to the target to as low as 10% of the kinetic energy flux of the freestream particles. As a consequence, the target is considerably cooler than the material within debris layer. However the detailed mechanisms of the formation of the debris layer and its subsequent interaction with the oncoming particles are still unresolved and require further investigation.

References

[1] Kuby, W. C. and Lewis, C. H., "An Experimental Study of the Effects of Particle Cloud Impingement," *AIAA Journal*, Vol. 6, No. 7, July 1968, pp. 1385–1387.

[2] Laderman, A. J., Lewis, C. H., and Byron, S. R., "Two Phase Plume Impingement Effects," *AIAA Journal* submitted for publication.

[3] Laderman, A. J. and Lewis, C. H., "Particle Cloud Impingement Damage," *Journal of Spacecraft and Rockets*, Vol. 6, No. 11, Nov. 1969, pp. 1327–1328.

[4] "Launch Vehicle Aerothermodynamic Design Assurance," Rept. D5-15441-2, Nov. 30, 1966, Space Div. Launch Branch, The Boeing Co.

Announcement: 1969 Author and Subject Indexes

The indexes of the four AIAA archive journals (*AIAA Journal, Journal of Spacecraft and Rockets, Journal of Aircraft,* and *Journal of Hydronautics*) will be combined, as they were in 1968, and mailed separately early in 1970. Subscribers are entitled to one copy of the index for each subscription which they had in 1969. Extra copies of the index may be obtained at $5 per copy. Please address your request for extra copies to the Circulation Department, AIAA, Room 280, 1290 Avenue of the Americas, New York, New York 10019.

Ruth F. Bryans
Director, Scientific Publications